SUPER-RESOLUTION IMAGE RECONSTRUCTION FROM ALIASED FLIR IMAGERY

S. Susan Young
Army Research Laboratory, Adelphi, MD 20783 USA

Ronald G. Driggers
Night Vision & Electronic Sensors Directorate, Fort Belvoir, MD 22060 USA

ABSTRACT

This paper presents a super-resolution image reconstruction from a sequence of aliased imagery. The sub-pixel shifts (displacement) among the images are unknown due to uncontrolled natural jitter of the imager. A correlation method is utilized to estimate sub-pixel shifts between each low resolution aliased image with respect to a reference image. An error-energy reduction algorithm is derived to reconstruct the high-resolution alias-free output image by imposing the spatial domain constraint and the spatial frequency domain constraint in an iterative fashion to form the desired alias-free (super-resolved) image. The results of testing the proposed algorithm on the simulated low resolution FLIR (Forward-Looking Infrared) images and real world FLIR images are provided.

1. INTRODUCTION

Many low-cost sensors spatially or electronically undersample an image. This results in aliased imagery in which the high frequency components are folded into the low frequency components in the image. Consequently, subtle/detail information (high frequency components) are lost in these images. An image/signal processing method, called super-resolution image reconstruction, can increase image resolution without changing the design of the optics and the detectors. In other words, super-resolution image reconstruction can produce high-resolution images by using the existing low-cost imaging devices from a sequence (or a few snapshots) of low resolution images. The emphasis of the super-resolution image reconstruction algorithm is to de-alias the undersampled images to obtain an alias-free or, as identified in the literature, a *super-resolved* image. This process also increases the image bandwidth which is limited by the imager post filter.

When undersampled images have sub-pixel shifts between successive frames, they represent different information from the same scene. Therefore, the information that is contained in undersampled image sequence can be combined to obtain an alias-free (high-resolution) image. Super-resolution image reconstruction from multiple snapshots provides far more detail information than any interpolated image from a single snapshot.

There are three major steps in super-resolution image reconstruction methods (Park, 2003; Schuler and Scribner, 2000; Borman and Stevenson, 1999). They are:

1) Acquiring a sequence of images from the same scene with sub-pixel shifts (fraction pixel displacements) among the images.
2) Estimating the sub-pixel (fraction pixel) shift or displacements among the images.
3) Reconstructing the high-resolution image.

In the first step, there are two types of methods to acquire low resolution images with sub-pixel shifts among them. One method is to have a controlled pixel displacement (Zalevsky, 2004). In this method, a special sensor or scanner (hardware) is designed to capture multiple images in a known pattern, where each image is captured by displacing the sensor in a known distance that is not a multiple of a pixel, but rather is a multiple of a pixel plus a known fraction of a pixel. Another method is to have a non-controlled pixel displacement, e.g. natural jitter. This paper considers the natural jitter which is more cost effective and practical. For example, in many applications, an imager is carried by a moving platform. In a rescue mission, the camera may be carried by a helicopter, or a moving vehicle. In a military reconnaissance situation, the camera may be carried by a person, an unmanned ground vehicle (UGV), or an unmanned aerial vehicle (UAV).

The second step is to estimate the sub-pixel shift or fraction pixel displacements. There are many methods that are addressed in the literature. Frame-to-frame motion detection based on gradient decent

Report Documentation Page

Form Approved
OMB No. 0704-0188

1. REPORT DATE **00 DEC 2004**	2. REPORT TYPE **N/A**	3. DATES COVERED **-**

4. TITLE AND SUBTITLE **Super-Resolution Image Reconstruction From Aliased Flir Imagery**	5a. CONTRACT NUMBER
	5b. GRANT NUMBER
	5c. PROGRAM ELEMENT NUMBER
6. AUTHOR(S)	5d. PROJECT NUMBER
	5e. TASK NUMBER
	5f. WORK UNIT NUMBER
7. PERFORMING ORGANIZATION NAME(S) AND ADDRESS(ES) **Army Research Laboratory, Adelphi, MD 20783 USA; Night Vision & Electronic Sensors Directorate, Fort Belvoir, MD 22060 USA**	8. PERFORMING ORGANIZATION REPORT NUMBER
9. SPONSORING/MONITORING AGENCY NAME(S) AND ADDRESS(ES)	10. SPONSOR/MONITOR'S ACRONYM(S)
	11. SPONSOR/MONITOR'S REPORT NUMBER(S)

12. DISTRIBUTION/AVAILABILITY STATEMENT
Approved for public release, distribution unlimited

13. SUPPLEMENTARY NOTES
See also ADM001736, Proceedings for the Army Science Conference (24th) Held on 29 November - 2 December 2004 in Orlando, Florida., The original document contains color images.

14. ABSTRACT

15. SUBJECT TERMS

16. SECURITY CLASSIFICATION OF:			17. LIMITATION OF ABSTRACT	18. NUMBER OF PAGES	19a. NAME OF RESPONSIBLE PERSON
a. REPORT **unclassified**	b. ABSTRACT **unclassified**	c. THIS PAGE **unclassified**	**UU**	**8**	

methods are most used (Horn and Schunk, 1981; Irani and Peleg, 1991). Most of these methods need to calculate the matrix inversion or use an iterative method to calculate the motion vectors. In this paper, we utilize a correlation method to explore the translational differences (shifts in x and y domains) of Fourier transforms of two images to estimate sub-pixel shifts between two low resolution aliased images.

The third step in super-resolution image reconstruction is to reconstruct the high-resolution image. Many methods have been proposed to solve the problem. There can be divided into two categories: directive non-uniform interpolation and non-directive inverse processing. Directive interpolation methods are described using spatial interpolation at the inter-pixel position (Peleg et al., 1987), using warping procedure (Chiang and Boult, 2000), and using weighted interpolation (Alam et al., 2000). In non-directive inverse processing methods, an observation model is formulated to relate the original high-resolution image to the observed low resolution images. The solution of high-resolution image is often obtained by inverting a matrix or an iterative procedure. The observation model can be formulated in either the spatial or frequency domain. The corresponding inverse methods are implemented in both domains. These methods are called regularized super-resolution approaches (Tom and Katsaggelos, 1995).

This paper outlines an iterative error-energy reduction method to reconstruct the high-resolution image. The algorithm utilizes a correlation method to estimate sub-pixel shifts among the members of the acquired image sequence. We begin with a signal model to relate the aliased images via gross shifts and sub-pixel shifts (Section 2.).

The knowledge of the location of each low resolution image in the upsampled grid (processing array) is the basis of an iterative error-energy reduction algorithm to reconstruct the high-resolution (alias-free) image (Section 3.). For this purpose, spatial domain constraints (knowledge of samples of aliased images and their locations on the upsampled array) and spatial frequency domain constraint (bandwidth) are imposed in an iterative fashion to form the desired alias-free (super-resolved) image.

In Section 4, we provide experimental results using simulated low resolution FLIR images and real world FLIR images where the sub-pixel shifts among frames are caused by natural jittering of the imager. Conclusion is provided in Section 5.

2. SHIFT ESTIMATION

An overview of the super-resolution image reconstruction algorithm is illustrated in Fig. 1. A sequence of original input low resolution images is passed into the gross shift estimation algorithm to estimate the overall shift of each frame with respect to a reference frame. The undersampled low resolution images are captured either by natural jitter or some kind of controlled motion of the camera. The images of successive frames contain not only the sub-pixel shifts but also the integer pixel shifts. Before estimating the sub-pixel shifts, the gross shifts among frames are compensated. After the gross-shifts are estimated, the input images are realigned. Then the sub-pixel shifts are estimated for each frame with respect to a reference frame. The error-energy reduction algorithm is applied to the low resolution input images with the estimated sub-pixel shifts among images to obtain the high-resolution (alias-free) output. The output is either a single high-resolution image that is generated from a sequence of low resolution images or a sequence of high-resolution images such as in a video sequence that are generated from multiple sequences of low resolution images.

The shifts between two images are estimated using a correlation method to explore the translational differences (shifts in x and y domains) of Fourier transforms of two images. The operation of the sub-pixel shift estimation is identical to the gross shift estimation. However, in order to achieve sub-pixel accuracy, the images are upsampled first. The upsampling is obtained by a Fourier windowing method (Young, 2004). In this Fourier windowing method, the zero-padding with a window is applied to the Fourier transform of the input image to have an alias-free upsampled image. Then the correlation method is applied to two upsampled Fourier transforms of two input images to estimate the shifts in sub-pixel accuracy.

An example of sub-pixel shift estimation from 16 frames is shown in Fig. 2. The sub-pixel shift of each frame with respect to a reference frame is illustrated in the Fig. 2. From this figure, we can see that the sub-pixel shifts among frames are randomly distributed in both x and y domains. The sub-pixel motion among frames is not controlled in a fixed pattern in this example.

3. ERROR-ENERGY REDUCTION RECONSTRUCTION ALGORITHM

In the error-energy reduction algorithm, the high-resolution image values are reconstructed by removing aliasing from low resolution images. The algorithm is based on the concept that the error-energy is reduced by imposing both spatial and spatial frequency domain constraints: samples from low-resolution images; bandwidth of the high-resolution alias-free output image. The error-energy reduction algorithm has been utilized in other signal processing applications. Some of the well known examples included the works by Papoulis (Papoulis, 1975), Gerchberg (Gerchberg, 1974), and Stark et. al. (Stark and Oskoui, 1989). Papoulis utilized the available information both in spatial and frequency domains to extrapolate the distribution of auto-correlation for spectral estimation. In Gerchberg's work, in order to achieve resolution beyond the diffraction limit, the spectrum of the reconstructed object is enhanced (expanded) by reducing the energy of the error spectrum from one snap-shot (not a sequence). In the work by Stark and his associates, they described the projection onto convex sets (POCS) approach to combine the spatial observation model from a controlled rotation or scan and spatial domain constraints to achieve a high-resolution image.

The main feature of this proposed error-energy reduction algorithm is that we treat the spatial samples from low resolution images as a set of constraints to populate an *over-sampled* processing array; the processing array is sampled above the desired output bandwidth. The estimated sub-pixel locations of these samples and their values constitute a spatial domain constraint. Furthermore, the bandwidth of the alias-free image (or the sensor imposed bandwidth) is the criterion used as a spatial frequency domain constraint on the over-sampled processing array. One may also incorporate other spatial or spatial frequency domain constraints that have been used by others; e.g., positivity of the image in the spatial domain. (This constraint is similar to the amplitude constraint that was used by Stark et. al.)

3.1 Image Acquisition Model

Fig. 3a shows the system model for acquiring an undersampled image in a one-dimensional case. Let $f(x)$ be the ideal target signature that is interrogated by the sensor. The measured target signature $g(x)$ by the sensor is modeled as the output of a Linear Shift Invariant (LSI) system whose impulse response is the sensor's point spread function (PSF), $h(x)$; this is also known as the sensor *blurring* function. The relationship between the measured target signature and the original target signature in the spatial frequency k_x domain is:

$$G(k_x) = F(k_x)\, H(k_x)$$

where $G(k_x)$, $F(k_x)$, and $H(k_x)$ are the Fourier transforms of $g(x)$, $f(x)$, and $h(x)$, respectively.

Fig. 3b shows the factors that dictate the bandwidth of the measured target signature. The bandwidth of the sensor's PSF is fixed and is determined by the support of the transfer function $H(k_x)$. The bandwidth of the ideal target signature depends on, e.g., the range of the target in FLIR, radar, sonar, visible light, etc. For a target at the short range, more details of the target are observable; in this case, the ideal target signature bandwidth is relatively large. For a target at the long range, the ideal target signature bandwidth is smaller. Two curves in Fig. 3b illustrate the bandwidths of the sensor and the ideal target signature. The wider one could be the bandwidth of the target or the sensor, or vise versa. The output bandwidth of the measured target signature is the minimum bandwidth of the ideal target signature and the sensor, that is,

$$B_o = \min(B_t, B_s)$$

where B_o, B_t, and B_s are the bandwidths of the output target signature, the ideal target signature and the sensor PSF, respectively. The proposed super-resolution image reconstruction algorithm cannot produce an image whose bandwidth exceeds B_o.

One of the issues in super-resolution image reconstruction is the number of the undersampled images that are required to recover the alias-free image. Let the sampling space of the original undersampled images be Δ_x. From an information-theory point of view, the sampling space of the output high-resolution image that is reconstructed from k frames (with distinct sub-pixel shifts) is $\frac{\Delta_x}{k}$ in one-dimensional imaging systems, and $(\frac{\Delta_x}{\sqrt{k}}, \frac{\Delta_y}{\sqrt{k}})$ in two-dimensional imaging systems. Theoretically, more frames should provide more information and, thus, larger bandwidth and/or higher resolution. However, the super-resolution image quality does not improve when the number of processed undersampled images exceeds a certain value. This is due to the fact discussed above that the bandwidth recovery is limited by the minimum of the bandwidths of the sensor or ideal target signature. Resolution is ultimately limited by diffraction and sensitivity is ultimately limited by eye noise.

3.2. Implementation of Error-Energy Reduction Reconstruction Algorithm

Let the bandwidth of the input undersampled (aliased) images be B_i. The bandwidth of the alias-free (high-resolution) output image is denoted as B_o. In order to recover the desired (alias-free) bandwidth, it is important to select a processing array with a sample spacing smaller than the sample spacing of the desired high-resolution image. In this case, the 2D FFT of the processing array yields a spectral coverage, B_p, that is larger than the bandwidth of the output image.

Fig. 4 shows a diagram of the error-energy reduction algorithm. In the first step, the processing array is initialized by populating the grids using the input images according to the estimates of the sub-pixel shifts. Then, we form the 2-D Fourier transform of this processing array. Its spectrum has a wider bandwidth than the true (desired) output bandwidth. Therefore, the spatial frequency domain constraint is applied, that is, replacing zeros outside the desired bandwidth. The next step is to perform the inverse 2-D Fourier transform of the resultant array.

The resultant inverse array is not a true image because the image values at the known grid locations are not equal to the original image values. Then the spatial domain constraint is applied, that is, replacing those image values at the known grid locations with the known original image values. The procedure continues until the n th iteration.

The use of the available information in the spatial and spatial frequency domains results in a reduction of the energy of the error at each iteration step. At the odd steps of the iteration, the error is defined by

$$e_{2n+1} = \sum_{(x,y)\in[X_p,Y_p]} [p_{2n+1}(x,y) - p(x,y)]^2$$

where $p(x,y)$ is the high-resolution alias-free image on the processing array (grid), $p_{2n+1}(x,y)$ is the reconstructed high-resolution image at the iteration $2n+1$.

In this paper, the condition of the error-energy reduction is examined by defining the following ratio:

$$SNR_{2n+1} = 10\log_{10}\left(\frac{\sum_{(x,y)\in[X_p,Y_p]}[p(x,y)]^2}{\sum_{(x,y)\in[X_p,Y_p]}[p(x,y) - p_{2n+1}(x,y)]^2}\right) \quad (1)$$

If $SNR_{2n+1} < SNR_{\max}$ (where $SNR_{\max}$ is a pre-assigned threshold value), and the maximum iteration is not reached, the iteration continues. If $SNR_{2n+1} > SNR_{\max}$, i.e., the stopping criterion is satisfied, the iteration is terminated. Before the final super-resolution image is generated, the bandwidth of the output image is reduced from B_p to B_o using the Fourier windowing method (Young, 2004). Then the final super-resolution image with the desired alias-free bandwidth is saved for the output.

4. RESULTS

In this section, we provide several examples to demonstrate the merits of the proposed super-resolution image reconstruction algorithm. The first example is to use the simulated low resolution undersampled images from a high resolution FLIR image. Because the sub-pixel shift information for these simulated low resolution images is pre-determined, we can test the accuracy of the proposed sub-pixel shift estimate algorithm and the error-energy reduction reconstruction algorithm. Then real world images of FLIR sensors are utilized to test the proposed algorithm and demonstrate the merits of the proposed algorithm.

4.1 Simulated Low Resolution FLIR Images

The original FLIR tank image is shown in Fig. 5a. The size of this image is 40 pixels in the vertical dimension and 76 pixels in the horizontal dimension. First, we up-sample this image using the Fourier windowing method (Young, 2004) by a factor of 4 to obtain a simulated high resolution image with a size of 160×304 as shown in Fig. 5b. Then the low resolution images are generated from this simulated high resolution image by sub-sampling; the starting sample point (shift) is randomly generated for each low resolution image.

The size of the low resolution image is 20×38. The resolution factor between the simulated high resolution image and the low resolution images is 8. The low resolution images are formed by sub-sampling every 8 pixels in both dimensions from the simulated high resolution image. The first samples of the 4 low resolution images in the high resolution upsampled image are at (1, 1), (3, 2), (2, 5), and (7, 3), that represent the sub-pixel shift locations. The low resolution images are sub-sampled from the simulated high resolution image based on the pre-described sub-pixel location points. For example, the simulated low resolution image No. 2 is formed by sub-sampling the simulated high resolution image starting at the 3^{rd} sub-pixel position in the first dimension and 2^{nd} sub-pixel position in the second dimension. Four simulated low resolution images are shown in Fig. 5c-f.

After applying the sub-pixel shift estimation algorithm to these 4 simulated low resolution images, the sub-pixel shift values are obtained. The estimated sub-pixel shift values are all correct according to the actual shifts.

The reconstructed image from the error-energy reduction algorithm is shown in Fig. 5j. For comparison purposes, we also applied a standard interpolation algorithm based on the gradient estimated sub-pixel shifts among these 4 low-resolution images. The resultant image is shown in Fig. 5i. This image shows artifacts that could be due to the fact that the sub-pixel shifts are not accurately estimated and the number of the input low resolution images is small (It is stated in the literature that these algorithms require a large number of snap shots (Schuler et al., 2002). The ratio of signal to error (defined in the equation (1)) between the high-resolution output image in Fig. 5i and the original image in Fig. 5a is 0.56dB. This indicates that the error between the high-resolution output image and the original image is large. Fig. 5g-h show one of the low-resolution images and its bilinear interpolated image. The ratio of signal to error between the bilinear interpolated image in Fig. 5h and the original image in Fig. 5a is 0.71dB. This indicates that the error between the interpolated low resolution image and the original image is also large. The ratio of signal to error between the super-resolved image in Fig. 5j and the original image in Fig. 5a is 40.1dB. This indicates that the image formed via the proposed algorithm is a good estimate of the original image. By observing Fig. 5j and Fig. 5h, we can see that the super-resolved image shows a significant improvement by exhibiting the detailed information, especially around the road wheel area, of the tank.

4.2 FLIR Images

A sequence of FLIR images of a foliage area is acquired using a FLIR sensor, Indigo Systems Merlin LWIR uncooled microbolometer thermographic camera. The sub-pixel shifts among the frames are due to the natural jitter of the camera. Sixteen low resolution frames are used to reconstruct the high-resolution (de-aliased) image with the resolution improvement factor of 4, as shown in Fig. 6b. For comparison, one of the bilinear interpolated low resolution images is shown in Fig. 6a. The reconstructed image in Fig. 6b shows a significant improvement by revealing high frequency information on the tree branches.

Next we consider a sequence of FLIR images of a pickup truck that is acquired using the same FLIR sensor that was mentioned above. Similarly, the natural jittering camera produces the sub-pixel shifts among the frames. Fig. 7a shows a bilinear interpolated image from one of the low resolution images. Fig. 7b shows the high-resolution pickup truck image that is reconstructed using 16 low resolution images. This reconstructed image again illustrates a significant improvement by exhibiting the detailed information on the cabin and window area of the truck which contains rich high frequency information.

5. CONCLUSION

This paper proposes an iterative error-energy reduction algorithm to reconstruct the high-resolution (alias-free) output image that utilizes a correlation method to estimate the sub-pixel shifts among a sequence of low resolution aliased imagery. The proposed super-resolution image reconstruction algorithm provides a possibility to produce high-resolution images by using low resolution images from existing low-cost imaging devices. Our numerical study has indicated that our super-resolution image reconstruction algorithm can produce high-resolution images using 4 frames (doubling the original sampling rate) to 16 frames (quadrupling the original sampling rate). Whereas most other super-resolution image reconstruction methods require over 100 frames to achieve a similar performance (Schuler, 2002). In addition to the accuracy and robustness (stability) of the solution of our algorithm, the ability to use a relatively small number of frames that are acquired at sub-pixel shifts (instead of a continuous camera motion that is also required by many of the existing algorithms) brings a flexibility that is crucial in practical scenarios (operational systems), e.g., the Army's weapon system that requires low memory and fast processing. A human observer study was performed (Krapels et. al., 2004) that demonstrated the performance improvement of the proposed super-resolution image reconstruction algorithm for undersampled FLIR imagers.

REFERENCES

Alam, M.S., Bognar, J. G., Hardie, R. C., and Yasuda, B. J., 2000: Infrared image registration and high-resolution reconstruction using multiple translationally shifted aliased video frames, *IEEE. Trans. Instrumentation and Measurement*, vol. 49, no. 5, pp. 915-923.

Borman, S. and Stevenson, R. L., 1999: Super-resolution from image sequences – A review, *Proc. 1998 Midwest Symp. Circuits and Systems*, pp. 374-378.

Chiang, M.C. and Boult, T. E., 2000: Efficient super-resolution via image warping, *Image and Vision Computing*, vol. 18, no. 10, pp. 761-771.

Gerchberg, R. W., 1974: Super-resolution through error energy reduction, *Optica Acta*, vol. 21.

Horn, B. K. P. and Schunk, B. G., 1981: Determining optical flow, *Artificial Intelligence*, 17: 185-203.

Irani, M. and Peleg, S., 1991: Improving resolution by image registration, *CVGIP: Graphical Models and Image Processing*, vol. 53 (3), 231-239.

Krapels, K., Diggers, R. G., Murrill, S., Schuler, J., Thielke, M., and Young, S. S., 2004: Super-resolution performance for undersampled imagers, *Proceedings of SPIE vol. 5407, Defense and Security Symposium (Formerly AeroSense)*.

Papoulis, A., 1975: A new algorithm in spectral analysis and band-limited extrapolation, *IEEE Trans. on Circuits and Systems*, vol. 22 (9), pp. 735- 742.

Park, S. C., Park, M. K., and Kang, M. G., 2003: Super-resolution image reconstruction: a technical overview, *IEEE Signal Processing Magazine*, pp. 21-36.

Peleg, S., Keren, D., and Schweitzer, L., 1987: Improving image resolution using subpixel motion, *Pattern Recognition Letters*, vol. 5, pp. 223 – 226.

Schuler, J. M. and Scribner, D. A., 2000: Dynamic sampling, resolution enhancement, and super resolution, in *Analysis of Sampled Imaging Systems*, Eds by R. H. Vollmerhausen and R. G. Driggers, pp. 125 – 138, SPIE Press – The International Society of Optical Engineering, Bellingham, Washington.

Schuler, J. M., Howard, J. G., Warren, P., and Scribner, D., 2002: TARID-based image superresolution," *Proceedings of SPIE, Vol. 4719, Infrared and passive millimeter-wave imaging systems; design, analysis, modeling, and testing*; 3-5 April 2002, Orlando, pp. 247-254.

Stark, H. and Oskoui, P., 1989: High-resolution image recovery from image-plane arrays, using convex projections, *J. Opt. Soc. Am. A*, vol. 6, no. 11, pp. 1715-1726.

Tom, B.C. and Katsaggelos, A. K., 1995: Reconstruction of a high-resolution image by simultaneous registration, restoration, and interpolation of low-resolution images, *Proc. of 1995 IEEE Int. Conf. Image Processing*, vol. 2, Washington, DC, Oct. 1995, pp. 539 – 542.

Young, S. S., 2004: Alias-free image subsampling using Fourier-based windowing methods, *Optical Engineering*, 43(4), 843-855.

Zalevsky, Z., Shamir, N., and Mendlovic, D., 2004: Geometrical superresolution in infrared sensor: experimental verification, *Optical Engineering*, 43(6), pp. 1401 – 1406.

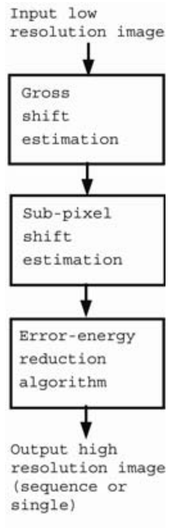

Fig.1 Overview of the super-resolution image reconstruction algorithm.

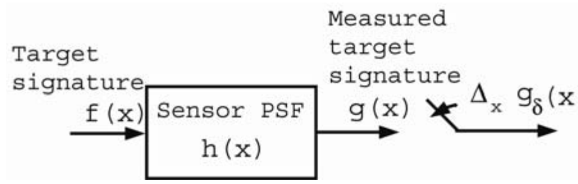

Fig. 3a Image acquisition model.

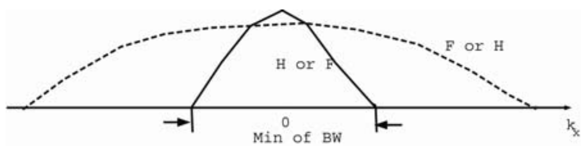

Fig.3b Factors that indicate the bandwidth of the measured target signature.

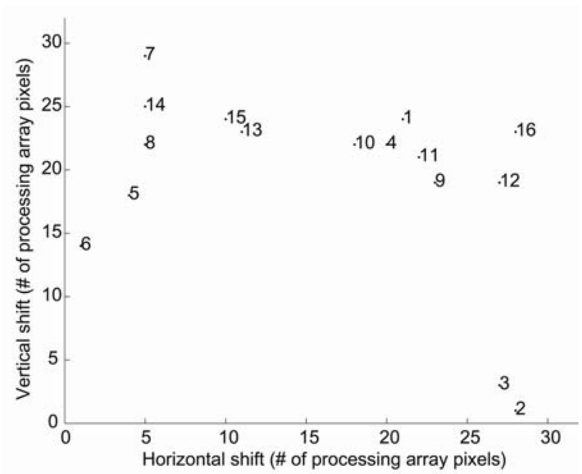

Fig.2 An example of sub-pixel shift estimation from 16 frames. The numbers on the figure represents the names of frames. The sub-pixel shifts of each frame with respect to a reference frame are illustrated at their corresponding sub-pixel locations.

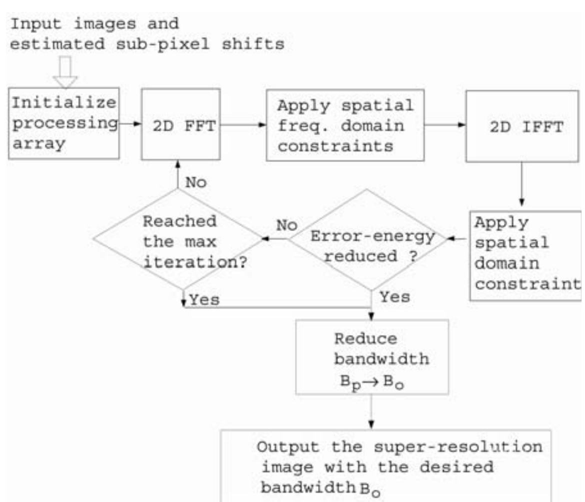

Fig. 4 Error-energy reduction algorithm.

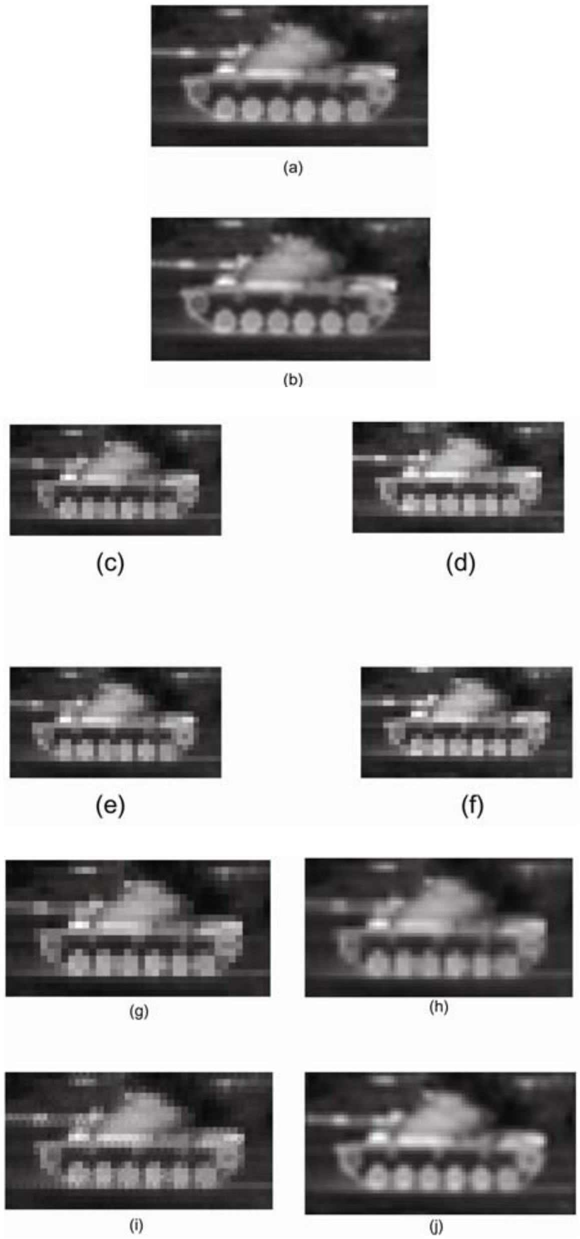

Fig. 5 Simulated low resolution FLIR images. (a) Original FLIR tank image. (b) Simulated high resolution image. (c) – (f) Four simulated low resolution images. (g) One of the simulated low resolution images. (h) One of the bilinear interpolated low resolution images. (i) High-resolution output image by the standard interpolation method based on the gradient estimated sub-pixel shifts. (j) Super-resolved image by the proposed algorithm.

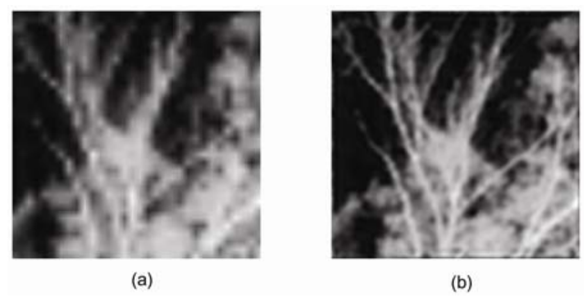

Fig. 6 FLIR images of a foliage area. (a) Bilinear interpolated image. (b) Super-resolved image by the proposed algorithm.

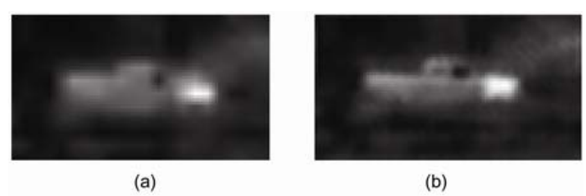

Fig. 7 FLIR images of a pickup truck. (a) Bilinear interpolated image. (b) Super-resolved image by the proposed algorithm.